# Modelling $q_{95}$ Windows for the Suppression of Edge Localized Modes by Resonant Magnetic Perturbations in the DIII-D Tokamak

R. Fitzpatrick

*Institute for Fusion Studies, Department of Physics,*

*University of Texas at Austin, Austin TX, 78712, USA*

## I. INTRODUCTION

Tokamak discharges operating in high-confinement mode (H-mode) [1] exhibit intermittent bursts of heat and particle transport, emanating from the outer regions of the plasma, that are known as "type-I edge localized modes" (ELMs).[2] It is estimated that the heat load that ELMs will deliver to the tungsten plasma-facing components in a reactor-scale tokamak, such as ITER, will be large enough to cause massive tungsten ion influx into the plasma core, and that the erosion associated with this process will unacceptably limit the lifetimes of these components.[3] Consequently, the development of robust and effective methods for ELM control is a high priority for the international magnetic fusion program.

The most promising method for the control of ELMs in H-mode tokamak discharges is via the application of static "resonant magnetic perturbations" (RMPs). Complete RMP-induced ELM suppression was first demonstrated on the DIII-D tokamak.[4] Subsequently, either mitigation or compete suppression of ELMs has been demonstrated on the JET,[5] ASDEX-U,[6] KSTAR,[7] MAST [8], and EAST [9] tokamaks.

The application of a static RMP, resonant in the pedestal region (i.e., the region of strong pressure and current density gradients characteristic of the edge region of an H-mode tokamak discharge), to an H-mode tokamak discharge is observed to give rise to two distinct phenomena.[10–14] The first of these is the so-called "density pump-out", which is characterized by a reduction in the electron number density in the pedestal region that varies smoothly with the amplitude of the applied RMP, is (usually) accompanied by a similar, but significantly smaller, reduction in the electron and ion temperatures, but is not associated with ELM suppression. The second phenomenon is "ELM suppression" itself, which occurs when the amplitude of the applied RMP exceeds a certain threshold value. ELM suppression is only observed to take place when $q_{95}$ (i.e., the safety-factor on the magnetic flux-surface that encloses 95% of the poloidal flux enclosed by the last closed flux-surface) takes values that lie in certain narrow windows.[13,14]

Numerical simulations made using the cylindrical, nonlinear, two-fluid, reduced-magneto-hydrodynamical (MHD), initial-value code, TM1 [15–17] have shed considerable light on the hitherto poorly understood physical mechanism that underlies RMP-induced ELM suppression in H-mode tokamak discharges.[18] The simulations in question make a plausible case that the density pump-out phenomenon is associated with the formation of locked (i.e.,

non-rotating) helical magnetic island chains at the bottom of the pedestal, whereas the ELM suppression phenomenon is associated with the formation of a locked helical magnetic island chain at the top of the pedestal. The prevailing hypothesis is that such an island chain suppresses ELMs by limiting the expansion of the pedestal, and, thereby, preventing it from attaining a width sufficient to destabilize peeling-ballooning modes [19] (which are thought to trigger ELMs).[20]

Recently, a toroidal generalization of the cylindrical asymptotic matching model presented in Ref. 21 was formulated and used to model RMP-induced ELM suppression experiments performed on the DIII-D tokamak,[22] leading to similar conclusions to the aforementioned TM1 studies. The primary aim of this paper is to employ this new model to try to account for the $q_{95}$ ELM suppression windows that are apparent when the edge safety-factor is slowly ramped in a particular DIII-D discharge in which an $n = 3$ RMP is used to control ELMs.[20,23]

It is well-known that magnetic reconnection caused when a (stable) tearing mode is driven by a static RMP that is resonant at a particular magnetic flux-surface in a tokamak plasma is facilitated when the associated "natural frequency" is relatively small.[24,25] The natural frequency of a (stable) tearing mode is the helical phase velocity that the mode would possess were it naturally unstable (in the absence of the RMP). Driven magnetic reconnection leads to the formation of a locked magnetic island chain at the resonant surface in question. Hence, the prevailing hypothesis is that a $q_{95}$ window for RMP-induced ELM suppression occurs when $q_{95}$ is such that the natural frequency of a tearing mode resonant at the top of the pedestal is close to zero. Unfortunately, there is currently some uncertainty in the fusion community regarding the form of the natural frequency.

According to linear tearing mode theory, a tearing mode is essentially convected by the local electron fluid at the resonant surface (see the discussion at the end of the Appendix).[26,27] Hence, if the response of an H-mode tokamak plasma to an applied RMP is governed by linear physics then we would expect the natural frequency to take the form [28–30]

$$\varpi_{\rm linear} = -n\,(\omega_E + \omega_{*\,e}), \tag{1}$$

where

$$\omega_E = -\frac{d\Phi}{d\Psi_p}, \tag{2}$$

$$\omega_{*\,e} = \frac{T_e}{e}\,\frac{d\ln p_e}{d\Psi_p}. \tag{3}$$

Here, $\Psi_p$ is the equilibrium poloidal magnetic flux (divided by $2\pi$), $\Phi(\Psi_p)$ the equilibrium scalar electric potential, $p_e(\Psi_p)$ the equilibrium electron pressure, $T_e(\Psi_p)$ the equilibrium electron temperature, $e$ the magnitude of the electron charge, and $n$ the toroidal mode number of the RMP. Moreover, the right-hand side of Eq. (1) is evaluated at the "rational" (i.e., resonant) magnetic flux-surface at which the safety-factor

$$q(\Psi_p) = \frac{d\Psi_t}{d\Psi_p}, \tag{4}$$

takes the rational value $n/m$, where $m$ is a positive integer. Here, $m$ and $n$ are the numbers of poloidal and toroidal periods, respectively, of the helical magnetic island chain driven at the rational surface. Furthermore, $\Psi_t(\Psi_p)$ is the equilibrium toroidal magnetic flux (divided by $2\pi$).

According to nonlinear tearing mode theory, a tearing mode is essentially convected by the local ion fluid at the rational surface (again, see the discussion at the end of the Appendix).[31–33] In fact, if the response of an H-mode tokamak plasma to an applied RMP is governed by nonlinear physics then we would expect the natural frequency to take the form [22]

$$\varpi_{\rm nonlinear} = -n\left(\omega_E + \left[1 - L_{00}^{ii} + L_{01}^{ii}\left(\frac{\eta_i}{1+\eta_i}\right)\right]\omega_{*\,i} - \left[L_{00}^{iI} - L_{01}^{iI}\left(\frac{\eta_I}{1+\eta_I}\right)\right]\omega_{*\,I}\right), \tag{5}$$

where

$$\omega_{*\,a}(\Psi_p) = -\frac{T_a}{Z_a\, e}\,\frac{d\ln p_a}{d\Psi_p}, \tag{6}$$

$$\eta_a(\Psi_p) = \frac{d\ln T_a}{d\ln n_a}, \tag{7}$$

for $a = i, I$. Here, $Z_i$, $n_i(\Psi_p)$, $T_i(\Psi_p)$, and $p_i(\Psi_p) = n_i\, T_i$ are the charge number, equilibrium number density, equilibrium temperature, and equilibrium pressure of the majority (thermal) ions, respectively, whereas $Z_I$, $n_I$, $T_I$, $p_I = n_I\, T_I$ are the corresponding quantities for the impurity ions. Furthermore, $L_{00}^{ii}(\Psi_p)$, $L_{01}^{ii}(\Psi_p)$, $L_{00}^{II}(\Psi_p)$, and $L_{01}^{II}(\Psi_p)$ are neoclassical parameters that are defined in Ref. 22. Note that these parameters are affected by charge exchange with neutrals. Finally, as before, the right-hand side of Eq. (5) is evaluated at the rational magnetic flux-surface.

A third possibility is that a tearing mode is convected by the local guiding center fluid at the rational surface,[14,34] in which case we would expect the natural frequency to take the

form

$$\varpi_{EB} = -n\,\omega_E. \tag{8}$$

As before, the right-hand side of Eq. (8) is evaluated at the rational magnetic flux-surface.

The secondary aim of this paper is to determine which of the three aforementioned choices for the natural frequency can best account for the $q_{95}$ ELM suppression windows observed in DIII-D.

## II. DESCRIPTION OF THEORETICAL MODEL

The theoretical model of the response of a tokamak plasma to an externally applied RMP that is employed in this paper is described in detail in Ref. 22. The model employs a standard asymptotic matching approch.[35–38] According to this approach, the response of the plasma to the applied RMP is governed by a combination of flux-freezing and perturbed force balance (this combination is often referred to as "marginally-stable ideal-MHD", which is a misnomer because MHD *per se* plays no role) everywhere in the plasma apart from a number of relatively narrow (in the radial direction) regions in which the applied perturbation resonates with the equilibrium magnetic field. Magnetic reconnection can take place within the resonant regions to produce relatively thin magnetic islands. Within the resonant regions, the plasma response is governed by nonlinear, as opposed to linear, two-fluid resistive MHD. This is the case because the widths of the magnetic island chains driven at the resonant surfaces exceed the linear layer widths (which invalidates linear theory).[21] Thus, when employing the asymptotic matching approach, the equations of flux-freezing and perturbed force balance are solved in the so-called "outer region" that comprises most of the plasma (and the surrounding vacuum), the equations of nonlinear two-fluid resistive-MHD are solved in the various resonant layers that constitute the so-called "inner region", and the two sets of solutions are then asymptotically matched to one another.

A toroidal tokamak equilibrium exhibits two distinct types of response to an applied RMP.[14,39,40] The first of these is known as the "tearing response"—this is a non-ideal-MHD response that is associated with the formation of current sheets and magnetic island chains at various resonant surfaces within the plasma. The second response type is known as the "kink response"—this is an edge-localized ideal-MHD response that is associated with coupling to a stable non-resonant kink mode. For the case of the tearing response, our model employs

an approximation in which the plasma response is assumed to be vacuum-like between the various resonant surfaces. On the other hand, the kink response of the plasma is calculated using the GPEC code.[41,42]

Our model has been implemented in the EPEC (Extended Perturbed Equilibrium Code) code. The name of this code reflects the fact that the nonlinear evolution of tearing modes in a tokamak plasma has far more in common with the $1\frac{1}{2}$-D evolution of the global plasma equilibrium than it does with conventional linear tearing mode physics. (See the discussion in the Appendix.) In particular, the Alfvén time is an irrelevant timescale in nonlinear tearing mode theory, and is also very much shorter than the timescales on which physical quantities of interest actually evolve. (Note that all timescales are normalized to the Alfvén time in Ref. 22. However, this is just a matter of convention. With the benefit of hindsight, it would have been better to normalize the timescales with respect to a diamagnetic timescale, in which case the Alfvén time would have completely dropped out of the final system of equations.)

## III. MODELING OF DIII-D DISCHARGE #145380

## IV. SUMMARY AND DISCUSSION

## ACKNOWLEDGEMENTS

This research was funded by the U.S. Department of Energy under contract DE-FG02-04ER-54742. The author would like to thank Q.M. Hu and R. Nazikian for providing the experimental data used in this paper.

## REFERENCES

[1] F. Wagner, G. Becker, K. Behringer, D. Campbell, A. Eberhagen, W. Engelhardt, G. Fussmann, O. Gehre, J. Gernhardt, G. v. Gierke, *et al.*, Phys. Rev. Lett. **49**, 1408 (1982).

[2] H. Zohm, Plasma Phys. Control. Fusion **38**, 105 (1996).

[3] A. Loarte, G. Saibene, R. Sartori, M. Bécoulet, L. Horton, T. Eich, A. Herrmann, M. Laux, G. Matthews, S. Jachmich, *et al.*, J. Nucl. Materials **313**–**316**, 962 (2003).

[4] T.E. Evans, R.A. Moyer, J.G. Watkins, P.R. Thomas, T.H. Osborne, J.A. Boedo, M.E. Fenstermacher, K.H. Finken, R.J. Groebner, M. Groth, *et al.*, Phys. Rev. Lett. **92**, 235003 (2004).

[5] Y. Liang, H.R. Koslowski, P.R. Thomas, E. Nardon, B. Alper, P. Andrew, Y. Andrew, G. Arnoux, Y. Baranov, M. Bécoulet, *et al.*, Phys. Rev. Lett. **98**, 265004 (2007).

[6] W. Suttrop, T. Eich, J.C. Fuchs, S. Günter, A. Janzer, A. Herrmann, A. Kallenbach, P.T. Lang, T. Lunt, M. Maraschek, *et al.*, Phys. Rev. Lett. **106**, 225004 (2011).

[7] Y.M. Jeon, J.-K. Park, S.W. Yoon, W.H. Ko, S.G. Lee, K.D. Lee, G.S. Yun, Y.U. Nam, W.C. Kim, J.-G. Kwak, K.S. Lee, H.K. Kim, and H.L. Yang, *et al.*, Phys. Rev. Lett. **109**, 035004 (2012).

[8] A. Kirk, I.T. Chapman, Y. Liu, P. Cahyna, P. Denner, G. Fishpool, C.J. Ham, J.R. Harrison, Y. Liang, E. Nardon, S. Saarelma, R. Scannell, A.J. Thornton, and MAST Team, Nucl. Fusion **53**, 043007 (2013).

[9] T. Sun, Y. Liang, Y.Q. Liu, S. Gu, X. Yang, W. Guo, T. Shi, M. Jia, L. Wang, B. Lyu, *et al.*, Phys. Rev. Lett. **117**, 115001 (2016).

[10] O. Schmitz, T.E. Evans, M.E. Fenstermacher, M. Lehnen, H. Stoschus, E.A. Unterberg, J.W. Coenen, H. Frerichs, M.W. Jakubowski, R. Laengner, *et al.*, Nucl. Fusion **52**, 043005 (2012).

[11] M.J. Lanctot, R.J. Buttery, J.S. de Grassie, T.E. Evans, N.M. Ferraro, J.M. Hanson, S.R. Haskey, R.A. Moyer, R. Nazikian, T.H. Osborne, *et al.*,
Nucl. Fusion **53**, 083019 (2013).

[12] C. Paz-Solden, R. Nazikian, S.R. Haskey, N.C. Logan, E.J. Strait, N.M. Ferraro, J.M. Hanson, J.D. King, M.J. Lanctot, R.A. Moyer, *et al.*, Phys. Rev. Lett. **114**, 105001 (2015).

[13] R. Nazikian, C. Paz-Soldan, J.D. Callen, J.S. de Grassie, D. Eldon, T.E. Evans, N.M. Ferraro, B.A. Grierson, R.J. Groebner, S.R. Haskey, *et al.*, Phys. Rev. Lett. **114**, 105002 (2015).

[14] C. Paz-Solden, R. Nazikian, L. Cui, B.C. Lyons, D.M. Orlov, A. Kirk, N.C. Logan, T.H. Osborne, W. Suttrop, and D.B. Weisberg, Nucl. Fusion **59**, 056012 (2019).

[15] Q. Yu, S. Günter, and B.D. Scott, Phys. Plasmas **10**, 797 (2003).

[16] Q. Yu, Nucl. Fusion **50**, 025014 (2010).

[17] Q. Yu, and S. Günter, Nucl. Fusion **51**, 073030 (2011).

[18] Q.M. Hu, R. Nazikian, B.A. Grierson, N.C. Logan, J.-K. Park, C. Paz-Soldan, and Q. Yu, Phys. Plasmas **26**, 120702 (2019).

[19] J.W. Connor, R.J. Hastie, H.R. Wilson, and R.L. Miller, Phys. Plasmas **5**, 2687 (1998).

[20] P.B. Snyder, T.H. Osboune, K.H. Burrell, R.J. Groebner, A.W. Leonard, R. Nazikian, D.M. Orlov, O. Schmitz, M.R. Wade, and H.R. Wilson, Phys. Plasmas **19**, 056115 (2012).

[21] R. Fitzpatrick, Phys. Plasmas **27**, 042506 (2020).

[22] R. Fitzpatrick, and A.O. Nelson, Phys. Plasmas **27**, 072501 (2020).

[23] Q.M. Hu, R. Nazikian, B.A. Grierson, N.C. Logan, D.M. Orlov, C. Paz-Solden, and Q. Yu, *The $q_{95}$ Windows of Edge-Localized-Mode Suppression using Resonant Magnetic Perturbations in the DIII-D Tokamak*, Phys. Rev. Lett., to appear (2020).

[24] R. Fitzpatrick, Nucl. Fusion **33**, 1049 (1993).

[25] R. Fitzpatrick, Phys. Plasmas **5**, 3325 (1998).

[26] R. Fitzpatrick, and T.C. Hender, Phys. Fluids B **3**, 644 (1991).

[27] A. Cole, and R. Fitzpatrick, Phys. Plasmas **13**, 032503 (2006).

[28] M. Bécoulet, F. Orain, P. Maget, N. Mellet, X. Garbet, E. Nardon, G.T.A. Huysmans, T. Casper, A. Loarte, P. Cayna, *et al.*, Nucl. Fusion **52**, 054003 (2012).

[29] N.M. Ferraro, Phys. Plasmas **19**, 056105 (2012).

[30] F. Orain, M. Bécoulet, G. Dif-Pradalier, G.T.A. Huysmans, S. Pamela, E. Nardon, C. Passeron, G. Latu, V. Grandgirard, A. Fil, *et al.*, Phys. Plasmas **20**, 102510 (2013).

[31] R. Fitzpatrick, and F.L. Waelbroeck, Phys. Plasmas **12**, 022307 (2005).

[32] R. Fitzpatrick, Phys. Plasmas **25**, 042503 (2018).

[33] R. Fitzpatrick, Phys. Plasmas **25**, 112505 (2018).

[34] M.F. Heyn, I.B. Ivanov, S.V. Kasilov, W. Kernbichler, I. Joseph, R.A. Moyer, and A.M. Runov, Nucl. Fusion **48**, 024005 (2008).

[35] H.P. Furth, J. Killeen, and M.N. Rosenbluth, Phys. Fluids **6**, 459 (1963).

[36] R. Fitzpatrick, R.J. Hastie, T.J. Martin, and C.M. Roach, Nucl. Fusion **33**, 1533 (1993).

[37] A.H. Glasser, Z.R. Wang, anf J.-K. Park, Phys. Plasmas **23**, 112506 (2016).

[38] R. Fitzpatrick, Phys. Plasmas **24**, 072506 (2017).

[39] S.R. Haskey, M.J. Lanctot, Y.Q. Liu, C. Paz-Soldan, J.D. King, B.D. Blackwell, and O. Schmitz, Plasma Phys. Control. Fusion **57**, 025015 (2015).

[40] D.A. Ryan, Y.Q. Liu, A. Kirk, W. Suttrop, B. Dudson, M. Dunne, R. Fischer, J.C. Fuchs, M. Garcia-Munoz, B. Kurzan, *et al.*, Plasma Phys. Control. Fusion **57**, 095008 (2015).

[41] J. K. Park, M.J. Schaffer, J.E. Menard, and A.H. Boozer, Phys. Rev. Lett. **99**, 195003 (2007).

[42] J.K. Park, and N.C. Logan, Phys. Plasmas **24**, 032505 (2017).

[43] R.J. Hawryluk, *Physics of Plasma Close to Thermonuclear Conditions: Vol. 1.* (Commission of the European Communities, Brussels, 1980.) Internal Document DUR-FU-BRU-XII/476180.

[44] R.D. Hazeltine, and J.D. Meiss, Rev. Mod. Phys. **121**, 1 (1985).

[45] P.H. Rutherford, Phys. Fluids **16**, 1903 (1973).

[46] J.A. Wesson, private communication (1993).

[47] R. Fitzpatrick, Phys. Plasmas **10**, 2304 (2003).

[48] G. Ara, B. Basu, B. Coppi, G. Laval, M.N. Rosenbluth, and B.V. Waddell, Ann. Phys. (N.Y.) **112**, 443 (1978).

[49] R. Fitzpatrick, P.G. Watson, and F.L. Waelbroeck, Phys. Plasmas **12**, 082510 (2005).

## Appendix A: Linear Versus Nonlinear Tearing Mode Theory in Tokamak Plasmas

The discussion in this Appendix outlines certain facts pertaining to tearing modes in tokamak plasmas that ought to be common knowledge in the magnetic fusion community (but appear not to be).

Consider a conventional tokamak plasma equilibrium. To lowest order, the equilibrium is governed by force balance,

$$-\nabla p + \mathbf{j}\times\mathbf{B} \simeq \mathbf{0}, \tag{A1}$$

and flux freezing,

$$\mathbf{E} + \mathbf{V}\times\mathbf{B} \simeq \mathbf{0}. \tag{A2}$$

This is the case because the other terms in the plasma equation of motion, (A1), and the plasma Ohm's law, (A2), are much smaller in magnitude than the retained terms. (Here, $p$ is the scalar pressure, $\mathbf{j}$ the current density, $\mathbf{B}$ the magnetic field strength, $\mathbf{E}$ the electric field strength, and $\mathbf{V}$ the plasma velocity). If we average the full plasma equation of motion and the full Ohm's law, as well as the full continuity and energy evolution equations, over magnetic flux-surfaces then the dominant terms in these equations are annihilated, and we end up with a set of $1\frac{1}{2}$-D evolution equations, according to which the magnetic field and plasma current evolve on the relatively long resistive timescale, $\tau_R$, whereas the density and temperature evolve on a somewhat shorter transport timescale.[43]

A linear tearing mode is a helical instability of a tokamak plasma equilibrium that is related to a shear-Alfvén wave.[44] The mode resonates with the plasma at the so-called rational magnetic flux-surface at which the shear-Alfvén velocity is zero. If $q$ is the safety-factor, $m$ the poloidal mode number, and $n$ the toroidal mode number, then the rational flux-surface is characterized by $q = m/n$. A thin resistive layer forms around the rational surface that permits the reconnection of magnetic flux on a much faster timescale than the global resistive evolution timescale, $\tau_R$, resulting in the formation of a helical magnetic island chain. Let the Alfvén time, $\tau_A$, be the typical timescale on which a (compressional) Alfvén wave traverses the plasma. In conventional tokamak plasmas, $\tau_A \ll \tau_R$. In fact, the magnetic Lundquist number, $S \equiv \tau_R/\tau_A$, typically exceeds $10^8$ in present-day tokamak plasmas, and will likely exceed $10^{10}$ in ITER plasmas. It turns out that the width of the resistive layer is typically a factor $S^{-2/5}$ smaller than the plasma minor radius, whereas magnetic flux is reconnected on the hybrid timescale $\tau_A \ll \tau_A^{2/5}\,\tau_R^{3/5} \ll \tau_R$.[35] Note that the structure of the tearing mode outside the resistive layer is simply governed by a combination of flux-freezing and perturbed force balance.

Figure 14 sketches the typical plasma current and vorticity patterns in a linear tearing layer. Observe that there is no distinction between a magnetic X-point and a magnetic O-point. The reason for this is that the magnetic separatrix of the reconnected magnetic island does not present an obstacle to plasma motion because the linear layer is so thin that the plasma can diffuse resistively across magnetic field-lines very rapidly. However, this is only the case as long as the radial width of the magnetic island chain is less than the linear layer width. As soon as magnetic reconnection at the rational surface has proceeded to such an extent that the magnetic island width exceeds the layer width then we enter the nonlinear

regime.

Figure 14 also sketches the typical plasma current and vorticity patterns in the nonlinear regime. Observe that there is now a considerable distinction between an X-point and an O-point. The reason for this is that the island is sufficiently wide that the plasma cannot diffuse across it resistively sufficiently rapidly to avoid being trapped inside the magnetic separatrix. Indeed, both the regions inside and outside the magnetic separatrix are governed by a combination of flux-freezing and perturbed force balance, whereas the resistive layer, within which the plasma can easily slip through the magnetic field, is diverted onto the magnetic separatrix. Moreover, as the island grows, the width of the separatrix layer becomes increasing negligible with respect to the island width. It turns out that the separatrix layer does not significantly affect the evolution of a nonlinear magnetic island chain. Indeed, the celebrated Rutherford island width evolution equation, which governs the evolution of the island width, is simply a $1\frac{1}{2}$-D evolution equation for a helical magnetic equilibrium localized around the rational surface.[45] The Alfvén time plays no role in this evolution (any more than it plays a role in the $1\frac{1}{2}$-D evolution of the global magnetic field). Likewise, the equation that determines the phase velocity of a nonlinear magnetic island chain (see Ref. 32, and references therein) is essentially an expression of the $1\frac{1}{2}$-D evolution of the plasma flow profiles across the island region. As before, the Alfvén time plays no role in this evolution (any more than it plays a role in the $1\frac{1}{2}$-D evolution of the global plasma flow profiles).

It follows, from the previous discussion, that the nonlinear evolution of a tearing mode in a tokamak plasma has far more in common with the $1\frac{1}{2}$-D evolution of the global plasma equilibrium than it does with conventional linear tearing mode physics. In particular, the Alfvén time is an irrelevant timescale in nonlinear tearing mode theory, and is also very much shorter than the timescales on which physical quantities of interest actually evolve. It should be noted that linear tearing layers in present-day tokamak plasmas are sufficiently thin that by the time a tearing mode is detectable it is already in the nonlinear regime (i.e., the island width exceeds the linear layer width).[46] It, therefore, makes very little sense to attempt to model tearing mode evolution in tokamak plasmas using a toroidal nonlinear magnetohydrodynamical (MHD) code. The reason for this is obvious: employing an MHD code necessarily introduces the very short Alfvén time into the calculation, but this timescale is actually irrelevant to the problem in hand. In fact, this is exactly the same reason that MHD codes are not usually used to reconstruct global plasma equilibria, or to model their

time evolution.

The natural frequency of a (stable) tearing mode is the helical phase velocity with which it would propagate were it actually unstable.[24] The natural frequency is determined by the equilibrium plasma flow at the rational surface. Now, a magnetic island is a helical pattern in the magnetic field generated by a helical current perturbation that is localized in the vicinity of the rational surface. Given that plasma current is predominately carried by the electrons, it is natural to suppose that a magnetic island chain (as well as the tearing mode perturbation away from the rational surface) is convected by the electron fluid in the immediate vicinity of the rational surface. This is indeed the case in the linear regime.[48] Of course, as a consequence of diamagnetic flows, if the island chain is convected by the electron fluid at the rational surface then it propagates with respect to the local ion fluid. However, this is not a problem because a linear layer is sufficiently thin that the magnetic field can diffuse through the plasma very rapidly, which implies that the ion fluid is not tied to the magnetic structure of the island chain. The situation is very different in the nonlinear regime. As we have seen, the region inside the magnetic separatrix of a nonlinear magnetic island chain is governed by a combination of flux-freezing and perturbed force balance. This implies that both the electron and the ion fluids are trapped inside the separatrix, and are, therefore, forced to co-rotate with the island chain. There is no such constraint outside the separatrix, so the electron and ion fluids rotate at different speeds in this region, as a consequence of diamagnetism. Consequently, one or other of the electron and the ion fluid rotation profiles must exhibit a strong gradient across the separatrix. The island propagation velocity is determined by which of the two fluids is most resistant to the formation of such a gradient. Of course, it is the ion fluid which is more resistant because of its much greater perpendicular viscosity,[31,49] as well as its much larger neoclassical stress tensor.[32] Hence, a nonlinear magnetic island chain is convected by the ion fluid in the vicinity of the rational surface, because this choice of propagation speed minimizes the ion fluid velocity gradient across the separatrix.

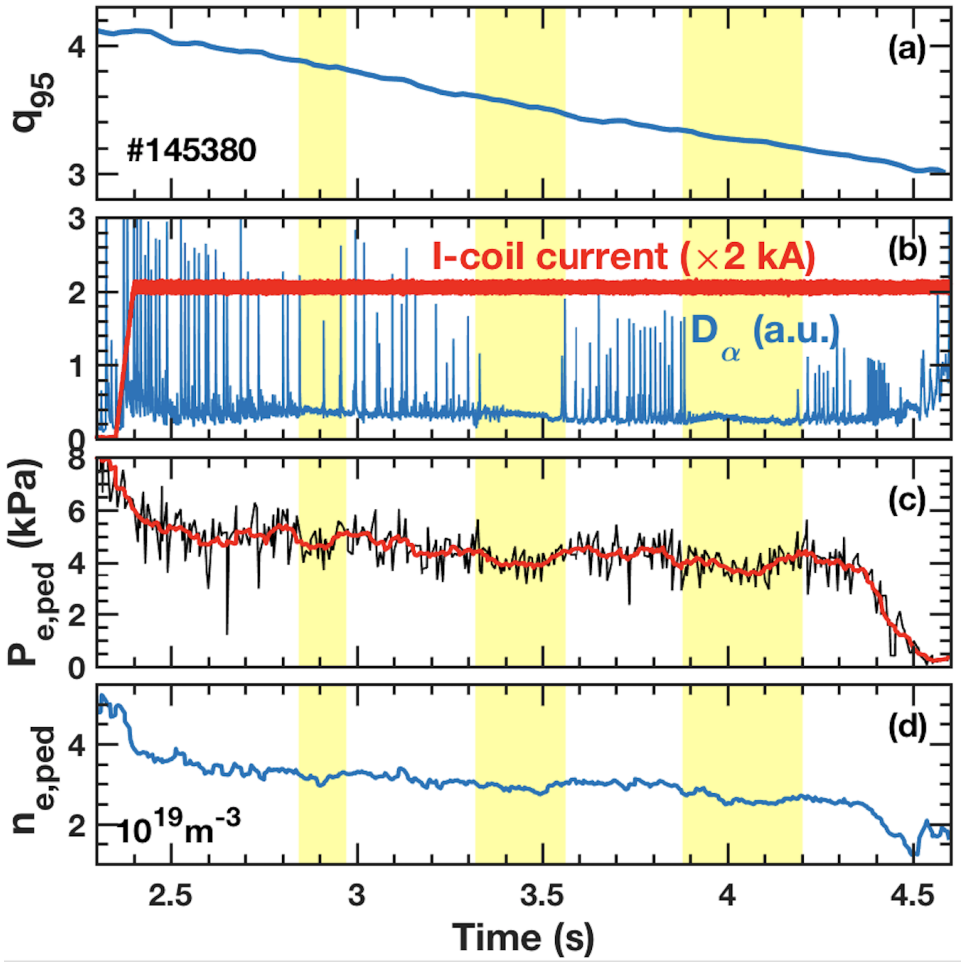


FIG. 1. Overview of DIII-D discharge #145380. (a) Safety factor at $\Psi_N = 0.95$. (b) $D_\alpha$ (i.e., Deuterium Balmer-alpha) signal, as well as $n = 3$ current flowing in upper and lower sections of I-coil. (c) Pedestal (i.e., $\Psi_N = 0.94$) electron pressure. (The red curve is the running average over 10 ms.) (d) Pedestal electron number density. The common vertical yellow bands indicate the ELM suppression windows.

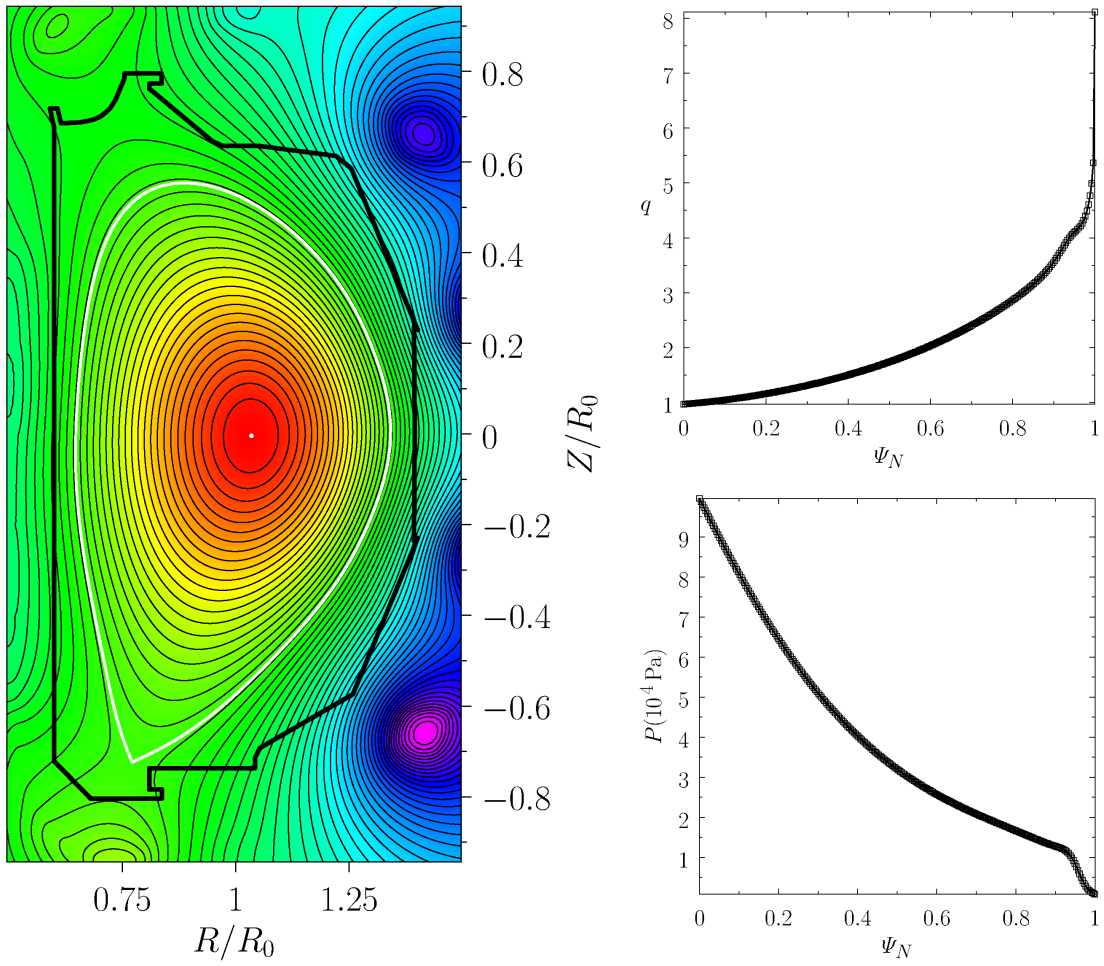


FIG. 2. Left Panel: Contours of the equilibrium poloidal magnetic flux in DIII-D discharge #145380 at time $t = 2500$ ms. The scale major radius is $R_0 = 1.70\,\mathrm{m}$. The white dot indicates the magnetic axis, the white curve indicates the last closed magnetic flux-surface, and the thick black line indicates the limiter. Upper-Right Panel: Safety-factor profile in DIII-D discharge #145380 at time $t = 2500$ ms. Lower-Right Panel: Total plasma pressure profile in DIII-D discharge #145380 at time $t = 2500$ ms.

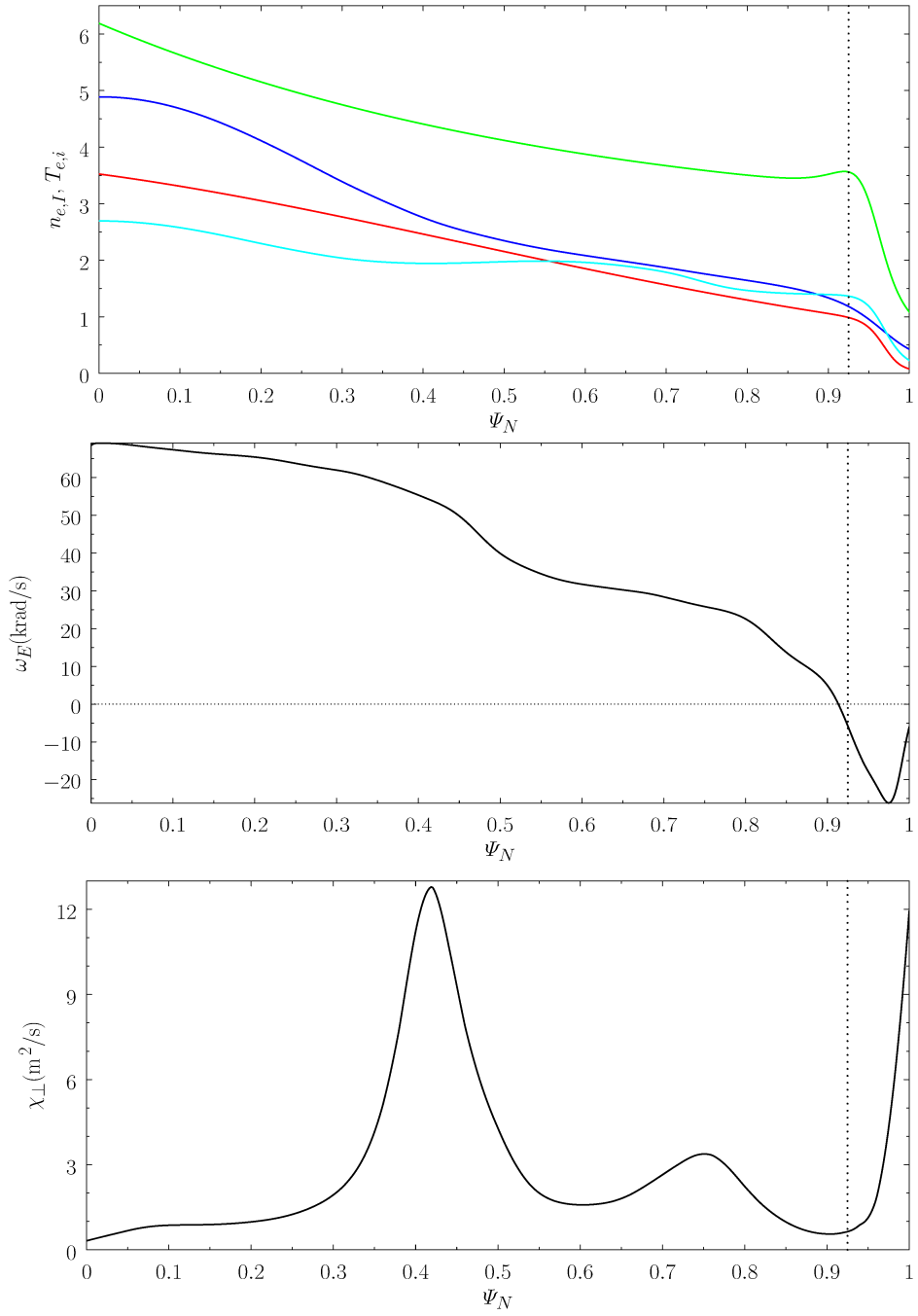


FIG. 3. Top Panel: The green, red, blue, and cyan curves show the electron number density ($10^{19}\,\mathrm{m}^{-3}$), electron temperature (keV), (thermal) ion temperature (keV), and C-VI ion number density ($10^{18}\,\mathrm{m}^{-3}$), profiles, respectively, in DIII-D discharge #145380 at time $t = 2500$ ms. Middle Panel: $\mathbf{E} \times \mathbf{B}$ frequency profile in DIII-D discharge #145380 at time $t = 2500$. Bottom Panel: Perpendicular momentum diffusivity profile in DIII-D discharge #145380 at time $t = 2500$ ms. The common vertical dotted lines indicate the location of the top of the pedestal, $\Psi_N = 0.925$.

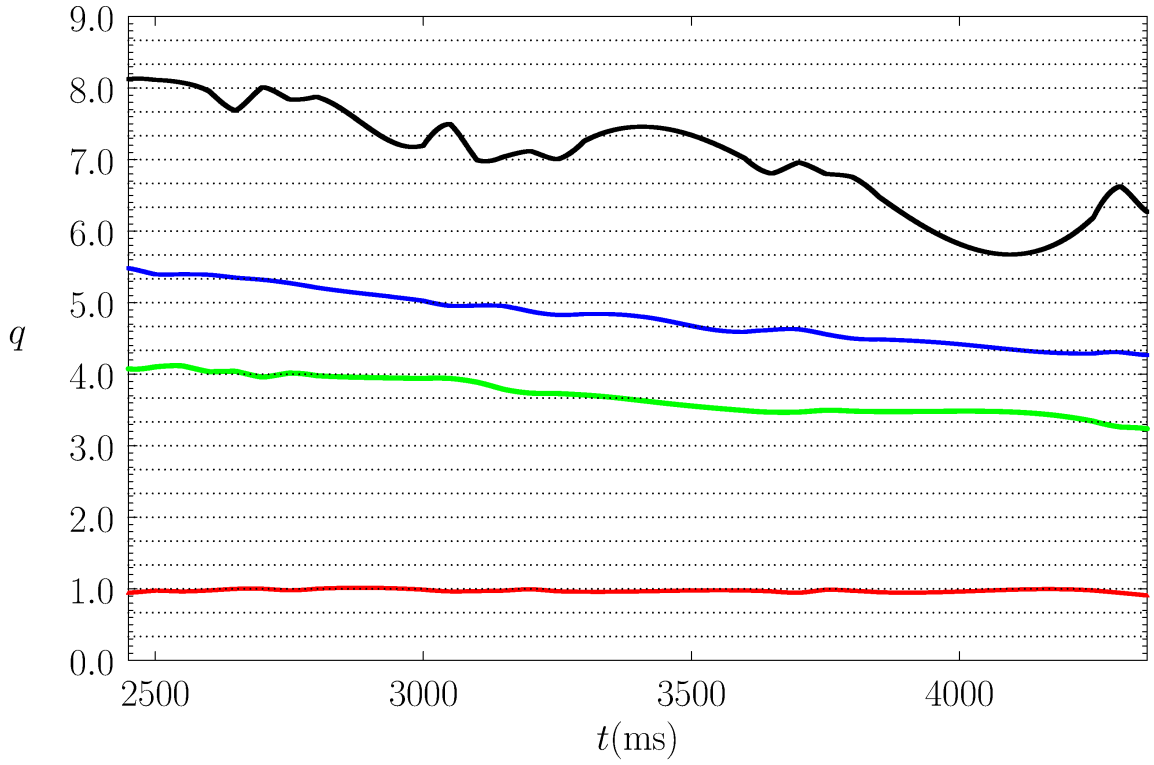


FIG. 4. Safety-factors as functions of time in DIII-D discharge #145380. The red, green, blue, and black curves show the safety-factors at the magnetic axis ($\Psi_N = 0.00$), the 95% flux surface ($\Psi_N = 0.950$), the effective plasma boundary for the GPEC and EPEC calculations ($\Psi_N = 0.997$), and the true plasma boundary ($\Psi_N = 1.00$), respectively. The horizontal dotted lines indicate the safety-factors at the various $n = 3$ rational surfaces.

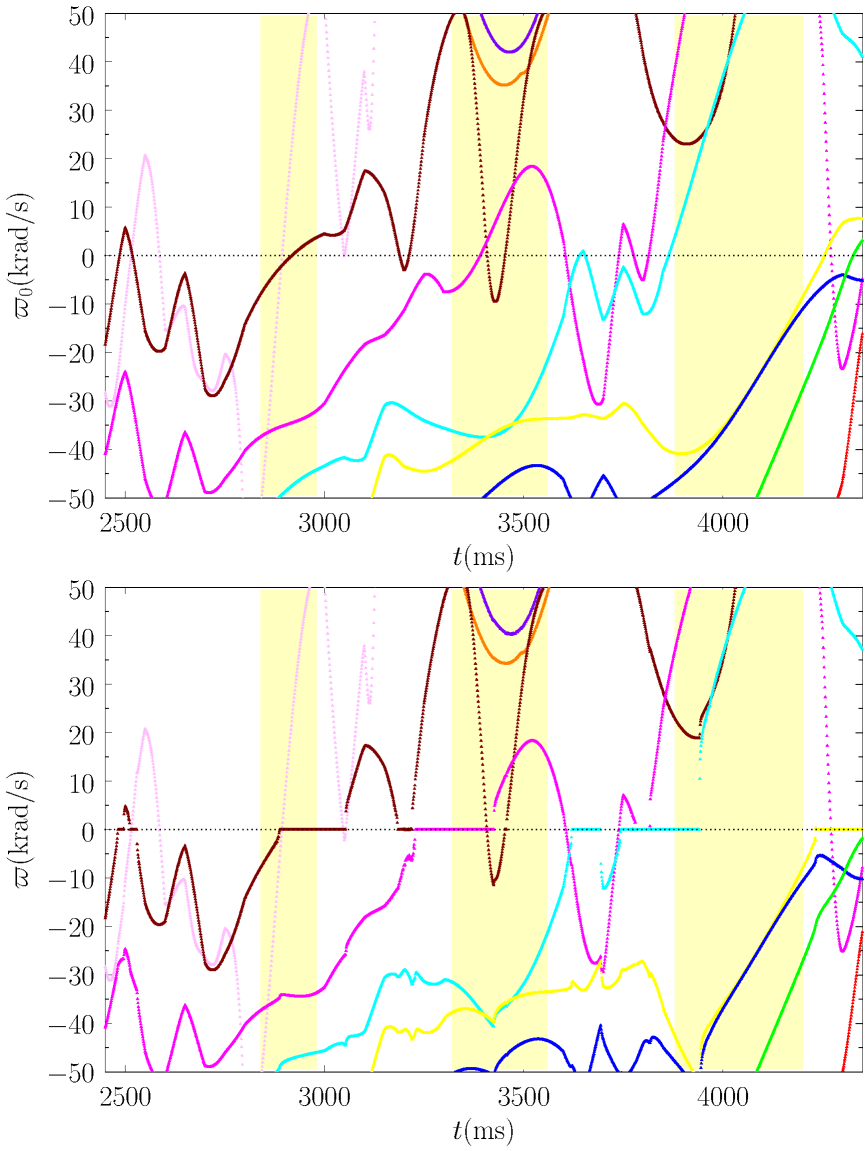


FIG. 5. Top Panel: $n = 3$ natural frequencies as functions of time in DIII-D discharge #145380, assuming that the natural frequency is determined by nonlinear island physics. Bottom Panel: $n = 3$ island frequencies as functions of time in DIII-D discharge #145380, assuming that the natural frequency is determined by nonlinear island physics. The red, green, blue, yellow, cyan, magenta, brown, pink, purple, and orange curves correspond to $m = 5$, 6, 7, 8, 9, 10, 11, 12, 13, and 14, respectively. The yellow vertical bands indicate the ELM suppression windows.

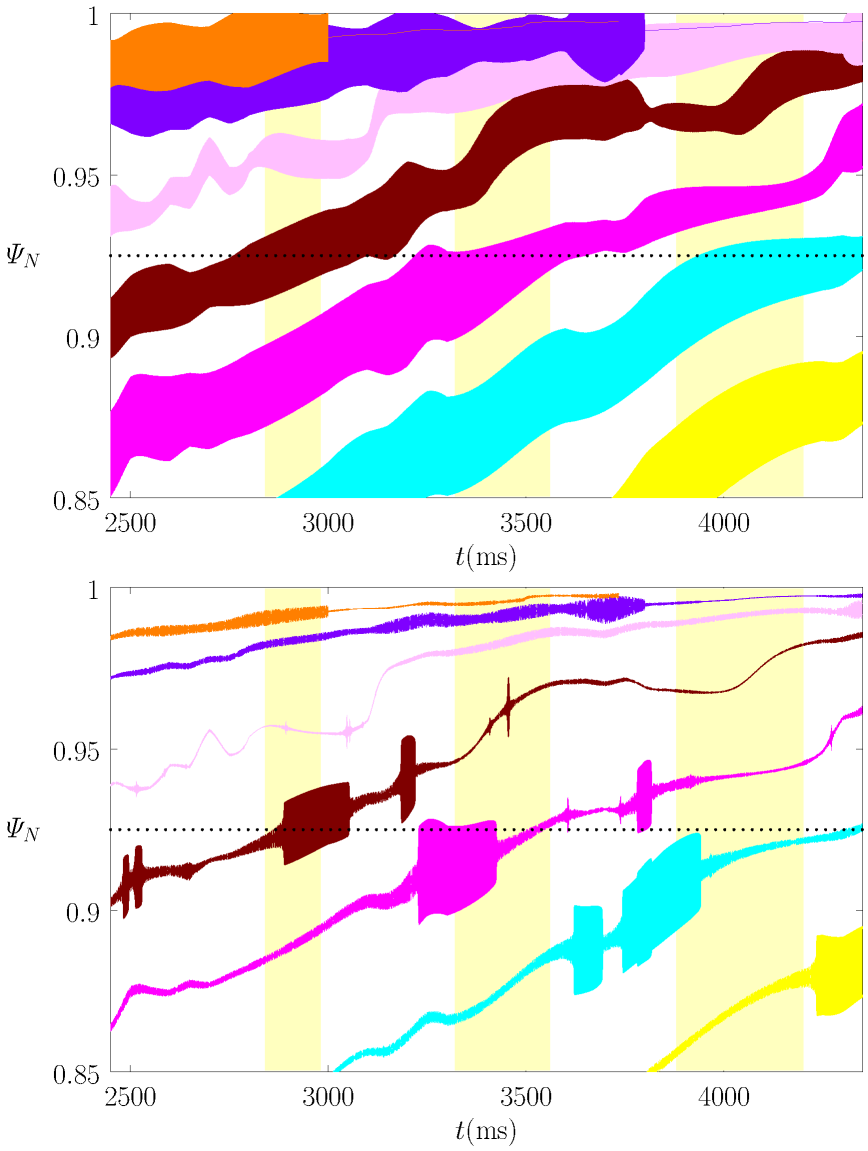


FIG. 6. Top Panel: Full $n = 3$ vacuum island widths as functions of time in DIII-D discharge #145380. Bottom Panel: Full $n = 3$ island widths as functions of time in DIII-D discharge #145380, assuming that the natural frequency is determined by nonlinear island physics. The blue, yellow, cyan, magenta, brown, pink, purple, and orange areas correspond to $m = 7$, 8, 9, 10, 11, 12, 13, and 14, respectively. The yellow vertical bands indicate the ELM suppression windows. The horizontal dotted lines indicate the top of the pedestal, $\Psi_N = 0.925$.

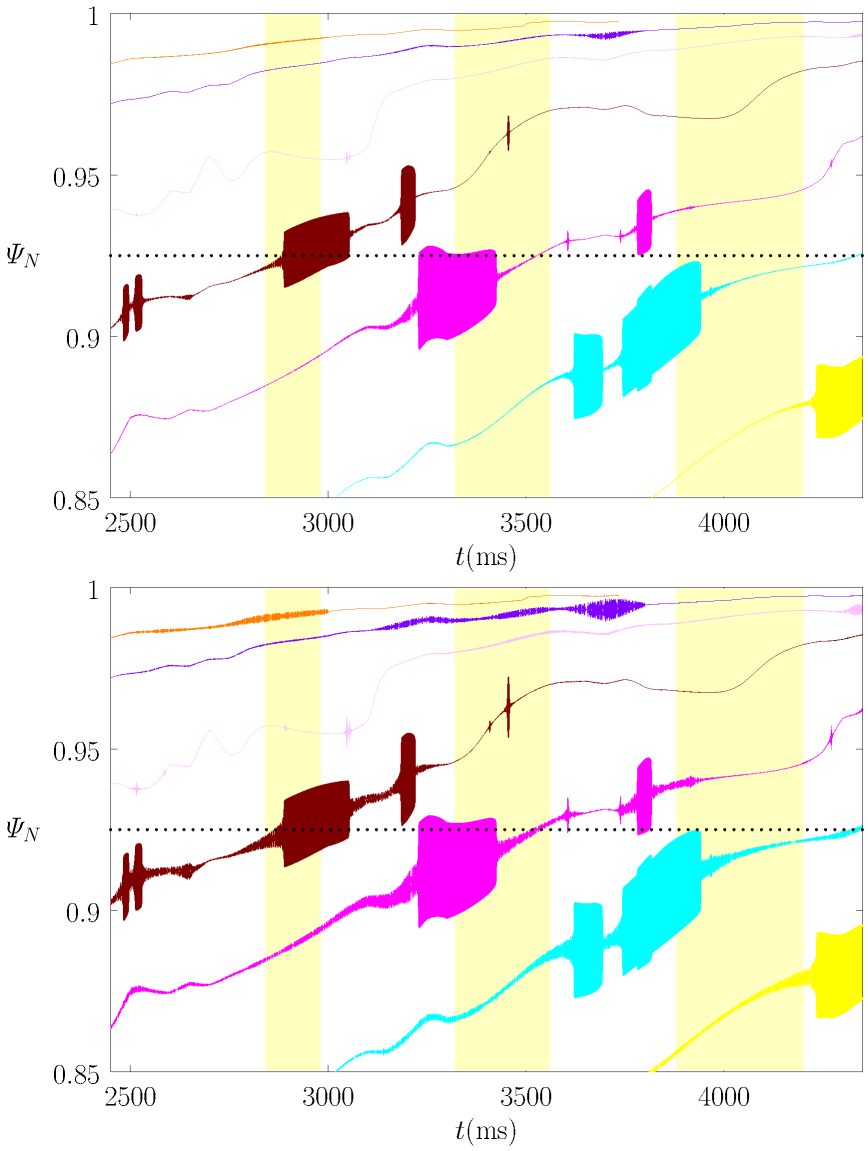


FIG. 7. Top Panel: Density flattening widths associated with induced $n = 3$ magnetic island chains as functions of time in DIII-D discharge #145380, assuming that the natural frequency is determined by nonlinear island physics. Bottom Panel: Electron temperature flattening widths associated with induced $n = 3$ magnetic island chains as functions of time in DIII-D discharge #145380, assuming that the natural frequency is determined by nonlinear island physics. The blue, yellow, cyan, magenta, brown, pink, purple, and orange areas correspond to $m = 7$, 8, 9, 10, 11, 12, 13, and 14, respectively. The yellow vertical bands indicate the ELM suppression windows. The horizontal dotted lines indicate the top of the pedestal, $\Psi_N = 0.925$.

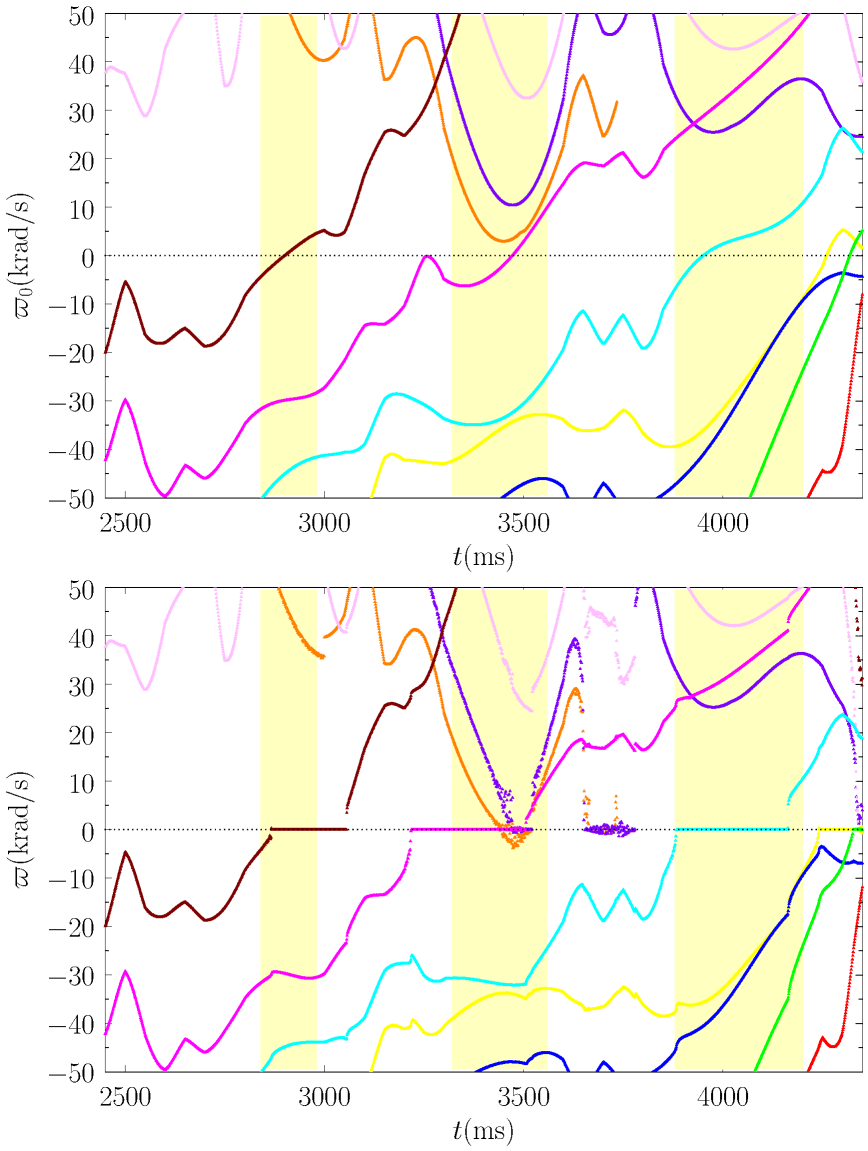


FIG. 8. Top Panel: $n = 3$ natural frequencies as functions of time in DIII-D discharge #145380, assuming that the natural frequency is coincident with the $\mathbf{E} \times \mathbf{B}$ frequency. Bottom Panel: $n = 3$ island frequencies as functions of time in DIII-D discharge #145380, assuming that the natural frequency is coincident with the $\mathbf{E} \times \mathbf{B}$ frequency. The red, green, blue, yellow, cyan, magenta, brown, pink, purple, and orange curves correspond to $m = 5$, 6, 7, 8, 9, 10, 11, 12, 13, and 14, respectively. The yellow vertical bands indicate the ELM suppression windows.

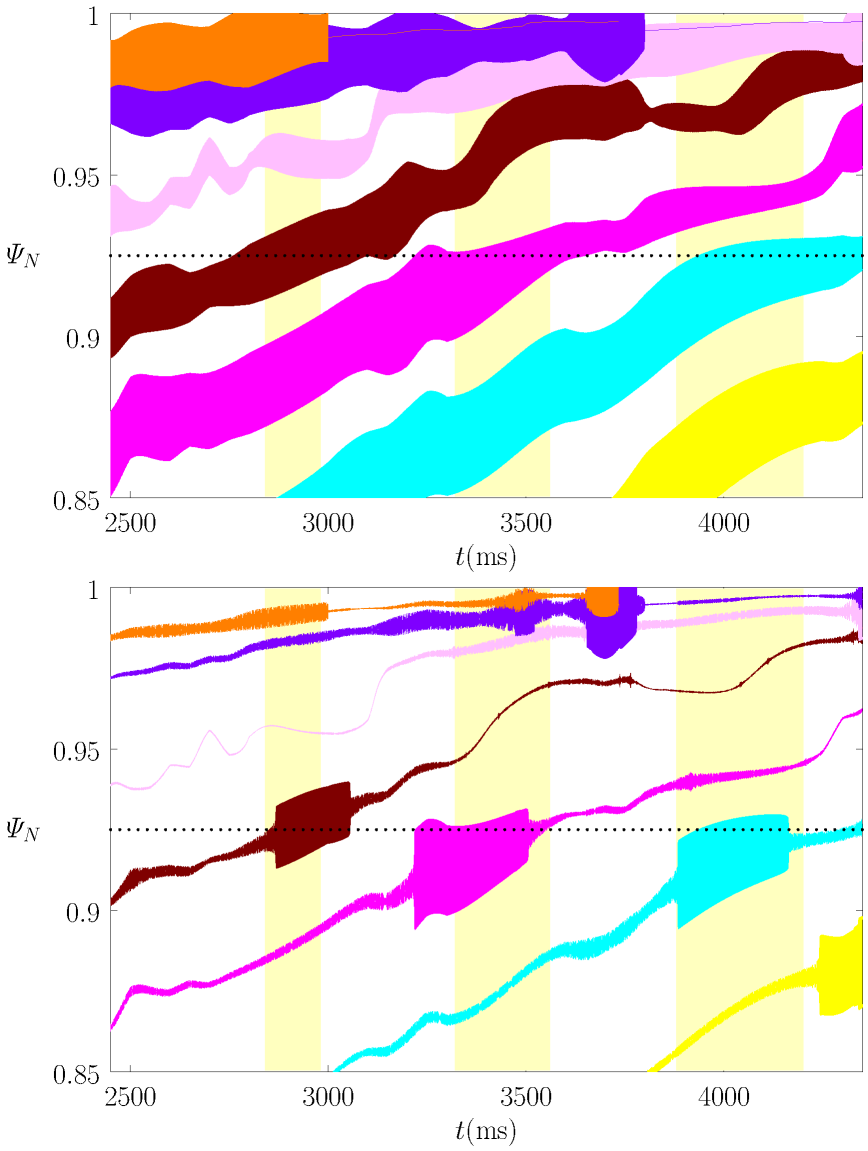


FIG. 9. Top Panel: $n = 3$ vacuum island widths as functions of time in DIII-D discharge #145380. Bottom Panel: $n = 3$ island widths as functions of time in DIII-D discharge #145380, assuming that the natural frequency is coincident with the $\mathbf{E}\times\mathbf{B}$ frequency. The blue, yellow, cyan, magenta, brown, pink, purple, and orange areas correspond to $m = 7$, 8, 9, 10, 11, 12, 13, and 14, respectively. The yellow vertical bands indicate the ELM suppression windows. The horizontal dotted lines indicate the top of the pedestal, $\Psi_N = 0.925$.

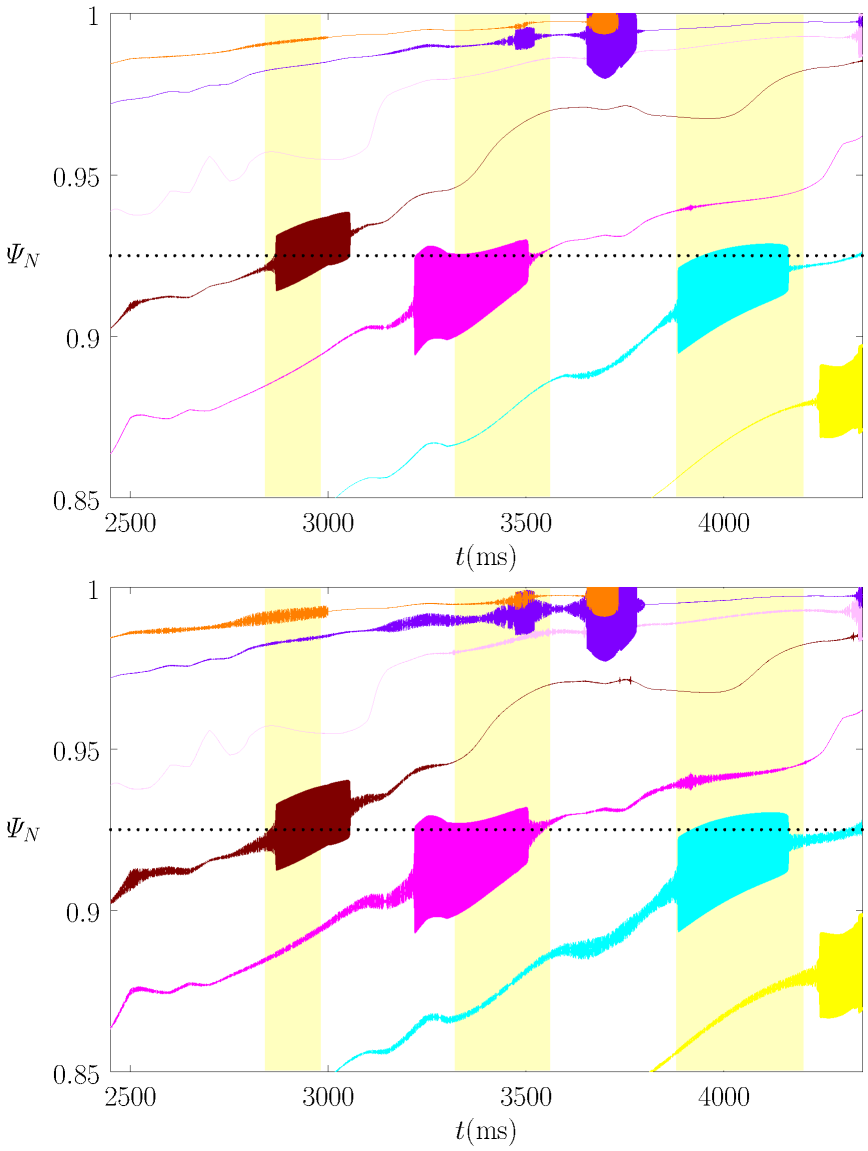


FIG. 10. Top Panel: Density flattening widths associated with induced $n = 3$ magnetic island chains as functions of time in DIII-D discharge #145380, assuming that the natural frequency is coincident with the $\mathbf{E} \times \mathbf{B}$ frequency. Bottom Panel: Electron temperature flattening widths associated with induced $n = 3$ magnetic island chains as functions of time in DIII-D discharge #145380, assuming that the natural frequency is coincident with the $\mathbf{E} \times \mathbf{B}$ frequency. The blue, yellow, cyan, magenta, brown, pink, purple, and orange areas correspond to $m = 7$, 8, 9, 10, 11, 12, 13, and 14, respectively. The yellow vertical bands indicate the ELM suppression windows. The horizontal dotted lines indicate the top of the pedestal, $\Psi_N = 0.925$.

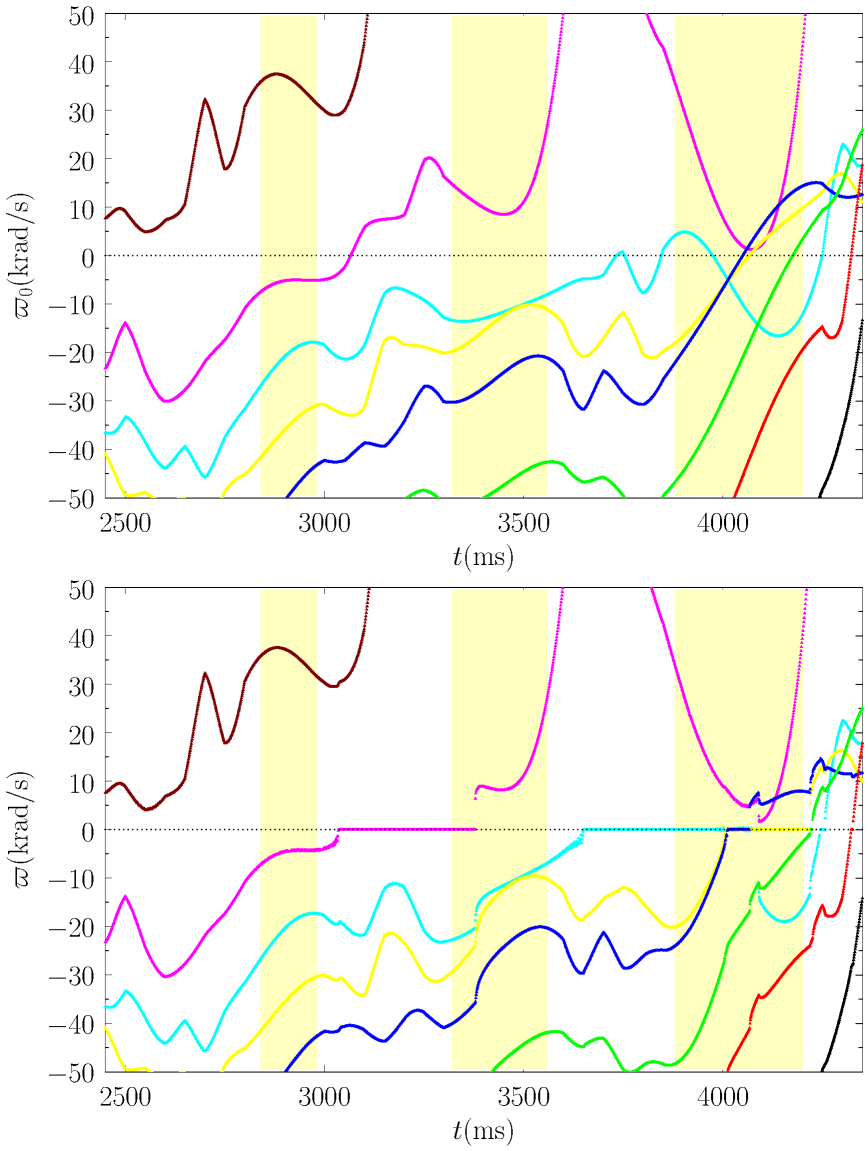


FIG. 11. Top Panel: $n = 3$ natural frequencies as functions of time in DIII-D discharge #145380, assuming that the natural frequency is determined by linear layer physics. Bottom Panel: $n = 3$ island frequencies as functions of time in DIII-D discharge #145380, assuming that the natural frequency is determined by linear layer physics. The black, red, green, blue, yellow, cyan, magenta, brown, purple, and orange curves correspond to $m = 4$, 5, 6, 7, 8, 9, 10, 11, 13, and 14, respectively. The yellow vertical bands indicate the ELM suppression windows.

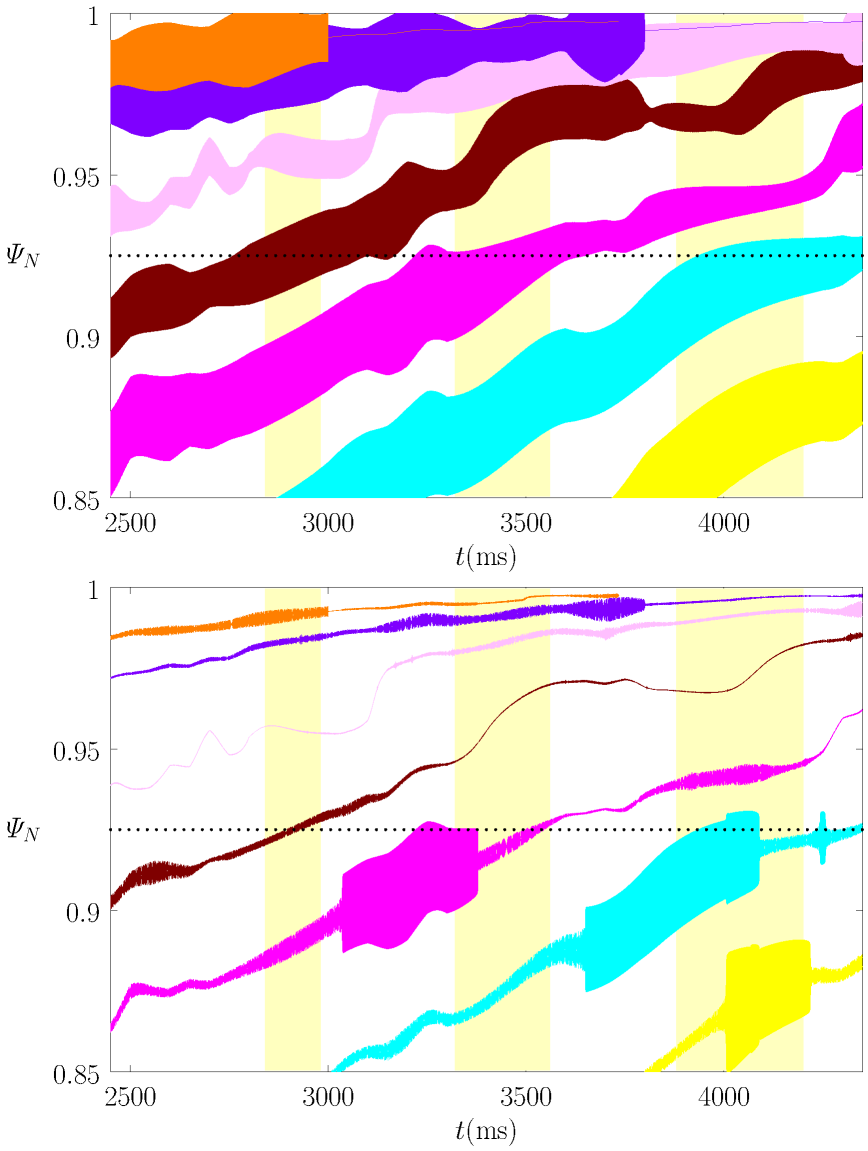


FIG. 12. Top Panel: $n = 3$ vacuum island widths as functions of time in DIII-D discharge #145380. Bottom Panel: $n = 3$ island widths as functions of time in DIII-D discharge #145380, assuming that the natural frequency is determined by linear layer physics. The blue, yellow, cyan, magenta, brown, pink, purple, and orange areas correspond to $m = 7$, 8, 9, 10, 11, 12, 13, and 14, respectively. The yellow vertical bands indicate the ELM suppression windows. The horizontal dotted lines indicate the top of the pedestal, $\Psi_N = 0.925$.

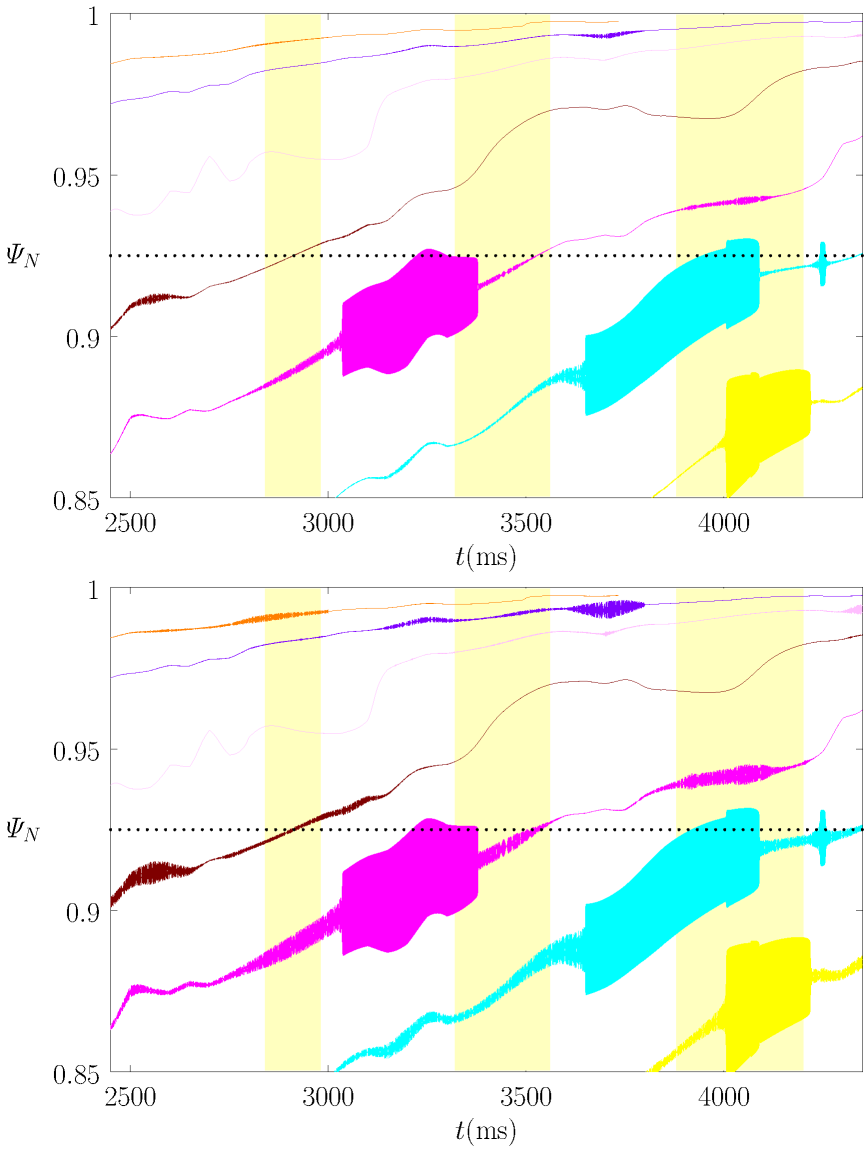


FIG. 13. Top Panel: Density flattening widths associated with induced $n = 3$ magnetic island chains as functions of time in DIII-D discharge #145380, assuming that the natural frequency is determined by linear layer physics. Bottom Panel: Electron temperature flattening widths associated with induced $n = 3$ magnetic island chains as functions of time in DIII-D discharge #145380, assuming that the natural frequency is determined by linear layer physics. The blue, yellow, cyan, magenta, brown, pink, purple, and orange areas correspond to $m = 7$, 8, 9, 10, 11, 12, 13, and 14, respectively. The yellow vertical bands indicate the ELM suppression windows. The horizontal dotted lines indicate the top of the pedestal, $\Psi_N = 0.925$.

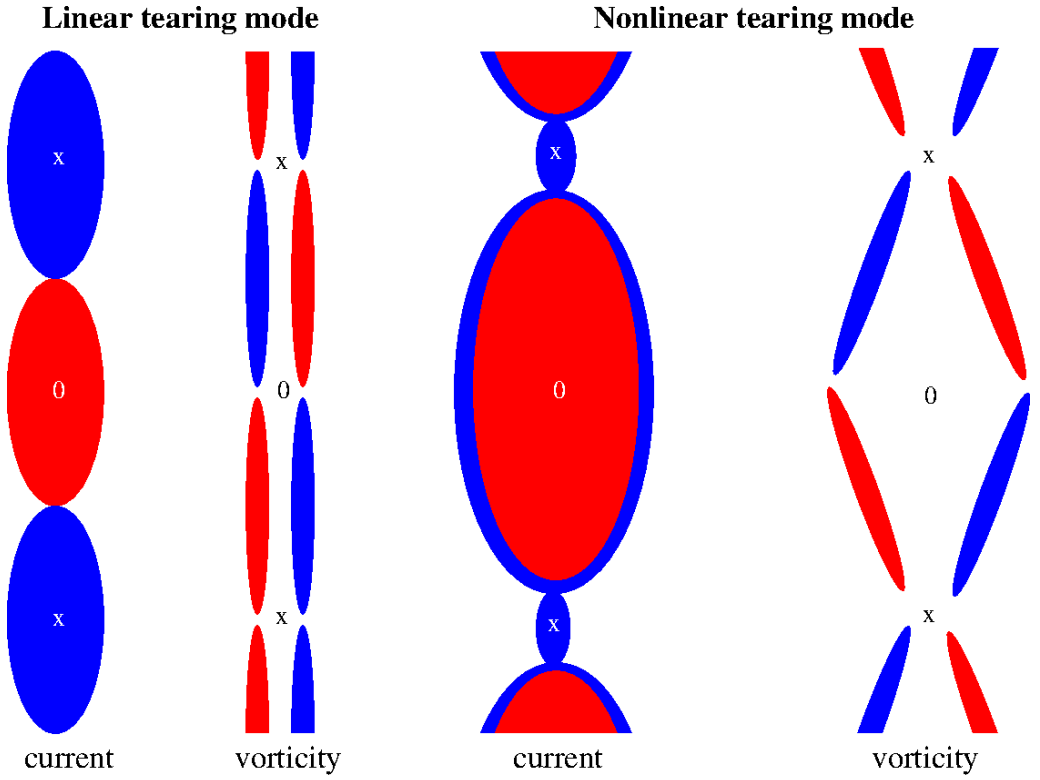


FIG. 14. Schematic diagram showing the perturbed plasma current and vorticity patterns around the magnetic X- and O-points of a linear and a nonlinear tearing mode. The horizontal axis measures radial distance from the rational surface, whereas the vertical axis measures distance along equilibrium magnetic field-lines. Red and blue correspond to positive and negative current/vorticity values, respectively. (See Figs. 7 and 10 in Ref. 47.)